ChemPubSoc Europe

DOI: 10.1002/cctc.201701133

CHEMCATCHEM Full Papers

Rapid Synthesis of Rhodium–Palladium Alloy Nanocatalysts

Graham W. Piburn, Hao Li, Pranaw Kunal, Graeme Henkelman,* and Simon M. Humphrey*[a]

The chemistry of metastable RhPd alloys is not well understood, and well-characterized nanoparticle (NP) examples remain rare. Well-defined and near-monodisperse RhPd NPs were prepared in a simple one-pot approach by using microwave-assisted or conventional heating in reaction times as short as 30 s. The catalytic hydrogenation activity of supported RhPd NP catalysts revealed that short synthesis times resulted in the most-active and most-stable hydrogenation catalysts, whereas longer synthesis times promoted partial Rh-Pd core–shell segregation. Relative to Rh NPs, RhPd NPs resisted deactivation over longer reaction times. Density functional theory (DFT) was employed to estimate the binding energies of H and alkenes on (111) Rh, Pd, and $Rh_{0.5}Pd_{0.5}$ surfaces. The DFT results concurred with experiment and concluded that the alkene hydrogenation activity trend was of the order Pd < RhPd < Rh. Rh-to-Pd charge-transfer in the RhPd alloys was found to play an important role in modulating the H binding energy.

Noble metals are widely used as catalysts in a variety of key industrial processes. In particular, rhodium is used to catalyze the reduction of NO_x to N_2 and O_2 in exhaust gas abatement and is also used in the conversion of bulk hydrocarbon feedstocks and syngas into more highly oxygenated hydrocarbons (e.g., hydroformylation).[1,2] Palladium also plays a myriad of critical roles, including CO-to-CO_2 oxidation in three-way catalytic converters and carbon–carbon bond-forming reactions.[1–3] Rh and Pd are also both widely employed in hydrogenation catalysis.[4–8] However, because of their scarcity in the Earth's crust, these metals are expensive to procure.[9] Whereas fundamental research into the possible replacement of noble-metal catalysts with cheaper, "Earth-abundant" transition-metal catalysts proceeds in earnest, large-scale industry continues to rely primarily on Pd, Rh, and other scarce noble-metal catalysts because their chemistry is reliable and well understood. Therefore, a major challenge is to increase the activity and selectivity of catalysts containing these metals, which will lead to greater product yields with lower energy consumption and the formation of fewer waste byproducts. Heterogeneous noble-metal catalysts can be made more efficient by designing their structures to suit the application at hand. Nanoparticle (NP) catalysts offer a significant improvement in atom efficiency over their bulk-metal counterparts because a far greater proportion of the metal atoms are at the surface of the material.[10] Compared to bulk grinding, so-called "bottom-up" synthesis methods using molecular precursors allow for greater control over the size and shape of the resulting NPs, which impacts both the number of accessible surface sites and their activity.[11–14] In addition to NP morphology effects, the composition of the material can also be tailored on the atomic level to better suit the desired reaction. Alloying two or more metals has been shown to allow for fine and continuous tunability of binding energies between the NP surface and substrates. This type of approach can even lead to a substantial enhancement in overall catalytic activity in cases in which one metal is unable to effect the catalysis on its own (e.g., RhAu or RhAg).[15–19]

This study focuses on determining fast (and therefore potentially scalable) and convenient means to prepare well-defined RhPd alloy NPs. The catalytic activity of the NPs was assessed by using cyclohexene hydrogenation as a model reaction, and the results were explored by using a state-of-the-art DFT approach. In the bulk phase, RhPd alloys can only be made by quenching mixtures of the two metals from co-melts heated above 1000 °C. Even upon formation under such harsh conditions, the kinetically trapped alloys are metastable and undergo segregation into the component pure metal phases upon adsorption of reactive species, that is, upon their use as heterogeneous catalysts.[20–23] However, previous work by Schaak and Kitagawa and their respective co-workers demonstrated that RhPd NPs could be made at much lower temperatures (95 °C).[24,25] In particular, Kitagawa and co-workers demonstrated that the NPs could resist segregation upon adsorption and desorption of H_2, presumably as a result of size-confinement effects at the nanoscale.[25] Their study showed that RhPd alloys reversibly stored and released hydride, which suggested to us that these materials should also be good candidates for hydrogenation catalysis.

Our continued interest in the application of microwave irradiation as a means to generate unusual bimetallic noble-metal NPs is based on the premise that metal-ion precursors and polar reducing polyol solvents both strongly couple with dipolar irradiation. This enables a unique heating profile that is well matched to NP nucleation and growth, in which it is possible to mimic high-temperature chemistry in nontoxic solvents through so-called "hotspot" generation, while avoiding the

[a] Dr. G. W. Piburn, H. Li, P. Kunal, Prof. G. Henkelman, Prof. S. M. Humphrey
Department of Chemistry, The University of Texas at Austin
2.204 Welch Hall, 105 E. 24th St. Stop A5300, Austin TX 78712 (USA)
E-mail: henkelman@utexas.edu
smh@cm.utexas.edu

Supporting Information and the ORCID identification number(s) for the author(s) of this article can be found under: https://doi.org/10.1002/cctc.201701133.

need for refluxing solvents.[26] Additionally, relative to conventional heating, microwave-assisted chemistry is more energy efficient and is suitable for continuous-flow synthesis.[19] As such, we are particularly interested to gain a better understanding of how synthesis time affects the resulting alloy NP structures and their catalytic reactivity, with the ultimate goal of minimizing synthesis time and concomitantly maximizing NP stability and reactivity.

It was shown previously in the microwave-assisted synthesis of PdAu alloy NPs that the most easily reducible metal (i.e., Pd) underwent near-instantaneous nucleation to form small (2 nm) NPs that subsequently facilitated random incorporation of less easily reducible Au atoms, which were autocatalytically reduced at the growing NP surfaces.[27] In this instance, after the metal-ion precursors were consumed, prolonged heating resulted in ripening to give fewer, larger alloy NPs. In the case of Rh^{III} and Pd^{II}, both metal ions tend to undergo facile reduction in hot ethylene glycol (EG) at approximately the same temperature ($\approx$90 °C).[28,29] As such, it appears that Rh and Pd undergo reduction and alloying in a single, fast step.

RhPd NPs were prepared by using an adapted version of our previously described experimental protocol employed to obtain RhX (X = Ag, Au) and PdAu binary alloy NPs. This method involves the use of simple, commercially available reagents and utilizes syringe-pump addition of precursors to ensure batch-to-batch reproducibility. Equimolar amounts of $RhCl_3$ and K_2PdCl_4 were dissolved in EG and injected at a rate of 12.5 mmol h^{-1} directly into a stirred solution of poly(vinylpyrrolidone) (PVP) in EG at 165 °C, either within a microwave cavity or by using an oil bath (conventional heating; see the Supporting Information). The total precursor injection time was 28 s, but the reaction mixture became black almost instantaneously upon precursor injection. The products were isolated (see the Supporting Information) at time intervals, t = 30 s, 3 min, 30 min and 3 h, after completion of the precursor-injection phase.

Transmission electron microscopy (TEM) imaging was used to study the morphology of the isolated RhPd NPs. For each set of conditions, a minimum of 300 NPs was measured from images obtained from two or more areas of the same grid. Representative TEM images and size distributions for the RhPd NPs synthesized under microwave irradiation are presented in Figure 1 a. In each case, the majority of NPs resembled truncated cubes, and the diameters exhibited narrow normal distributions (1σ). Interestingly, in comparison to previous observations for other bimetallic NPs prepared by using the same protocol, all RhPd NPs displayed very similar mean diameters and standard deviations [(5.0–5.2 ± 0.7–0.9) nm for the microwave-irradiated (μwl)-NPs; (5.4–5.8 ± 0.8–1.0) nm for the conventionally heated (CvH)-NPs, Figure S2 in the Supporting Information] regardless of heating time or the heating method employed. Evidently, NP ripening did not occur for the RhPd NPs, even after prolonged heating at 165 °C. Monometallic Rh NPs prepared by using a nearly identical method exhibited clear ripening effects in the presence of similar quantities of the capping agent PVP;[30] however, Pd NPs prepared by the same method at 165 °C underwent negligible ripening (Figure S3). Therefore,

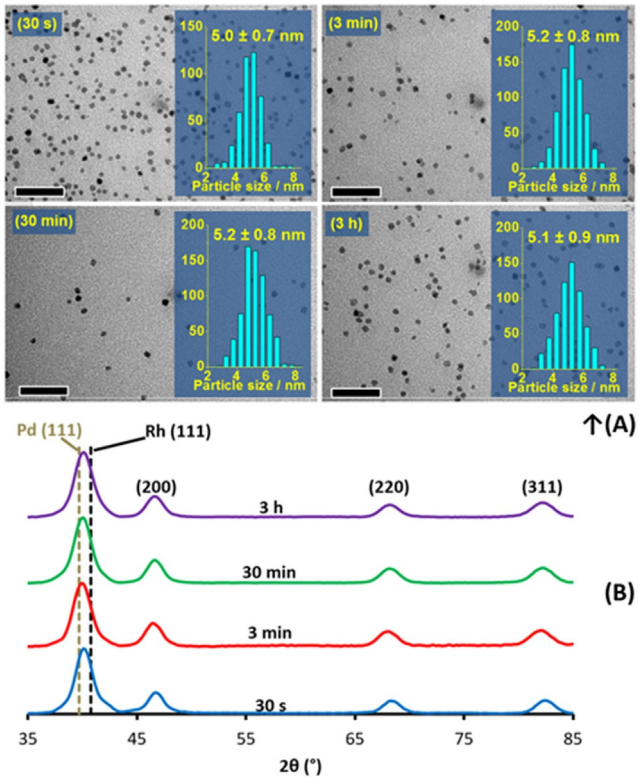

Figure 1. a) Representative TEM images and size distributions for μwl-RhPd NPs isolated from each of the four reaction times. b) Corresponding PXRD patterns; reference lines for the (111) peaks of pure Rh and Pd were obtained directly from PXRD of monometallic NPs synthesized by similar methods (see Figure S4).

the lack of significant growth of the RhPd NPs may plausibly be attributed to tuning of the binding energies between the NP surface and the Lewis donor groups of the PVP (amine R_3N or carbonyl C=O) closer to the binding energies for Pd NPs, which would disfavor further growth. This mechanism would be consistent with DFT calculations for cyclohexene and hydrogen binding energies (see below).

X-ray powder diffraction (XRPD) was used to analyze the bulk crystallinity of the RhPd NPs. Particles from all reaction conditions produced diffraction patterns matching face-centered cubic (FCC) lattice structures. The major reflections observed have 2θ values that lie between the corresponding reference peaks for pure FCC Rh and Pd as predicted from Vegard's law, which is indicative of random alloying of Rh and Pd (Figure 1 b, Figure S5, Table S6). Application of the Scherrer equation to the (111) reflection in each pattern (using a shape factor of 0.94[31]) resulted in estimated crystallite sizes that were consistently smaller than the measured average diameters by 0.5–1.0 nm (Table S7), which may indicate that a fraction of the NPs contains two or more crystalline domains. The 30 s samples for each heating method had the smallest discrepancies between the Scherrer estimate and the measured average, and the discrepancies were larger for the conventionally heated samples than the microwave heated ones.

The elemental composition of the RhPd alloy NPs was further probed by using a combination of X-ray photoelectron

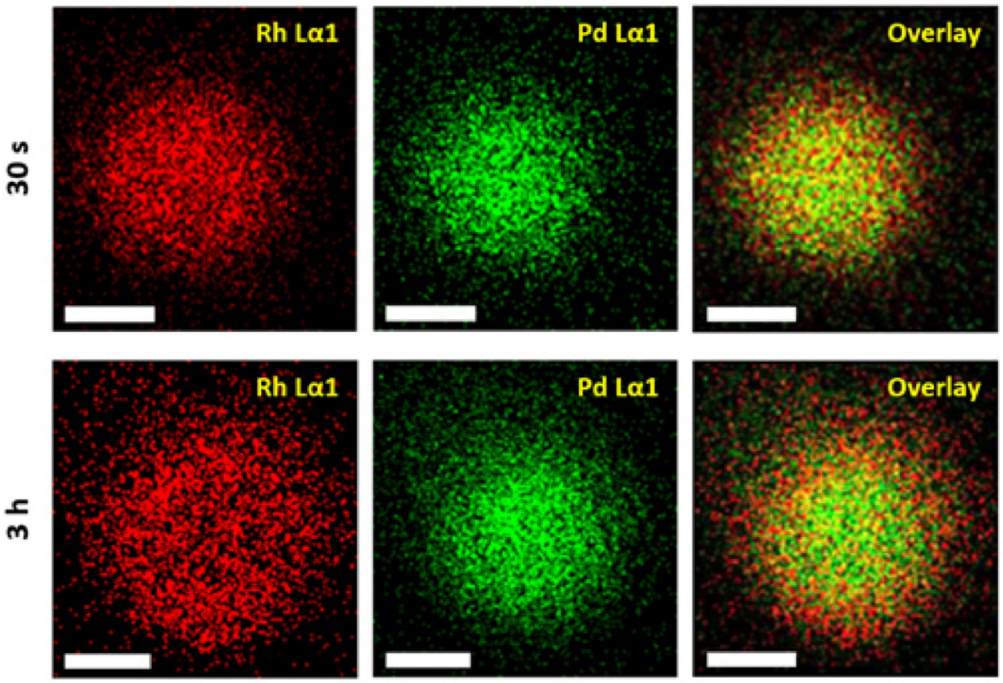

Figure 2. EDXS maps highlighting the distribution of Rh (red, left) and Pd (green, center) within single representative RhPd NPs made by using microwave reaction times of 30 s (top) and 3 h (bottom); the overlay of the two elements is shown on the right.

spectroscopy (XPS), inductively coupled plasma optical emission spectrometry (ICP-OES), and energy-dispersive X-ray spectroscopy (EDXS) in high-angle annular dark field scanning mode (HAADF-STEM). XPS showed that the μwI-NPs contained Rh/Pd ratios close to 1, with a slight (5–8%) excess of Pd for samples prepared in 30 s to 30 min, whereas prolonged heating for 3 h resulted in detection of more equimolar amounts of each metal (Figure S8 and Tables S9 and S11). In terms of the measured oxidation states, the proportion of Rh^{I} was lowest in the sample heated for only 30 s (25%) and increased to approximately 56% after 3 h. In contrast, the 30 s sample had one of the highest proportions of Pd^{II} (66%), and that value decreased over time to 45% after 3 h (Table S9); this may be indicative of the surface becoming enriched in rhodium at longer reaction times (see below). The elemental compositions provided by ICP-OES were in close agreement, and they indicated a slight excess amount of Pd in most cases (Tables S10 and S11).

In an attempt to probe the extent of homogeneity in individual RhPd NPs, EDXS mapping experiments were performed on the samples prepared by microwave irradiation with reaction times of 30 s to 3 h (Figure 2). Signals for both Rh and Pd were detected in every particle tested, and both were distributed throughout each particle. However, upon closer inspection, some important structural features were observed as a function of reaction time: the 30 s products showed a very even distribution of Rh and Pd throughout each NP (Figure 2, top), but NPs prepared by 3 h heating clearly showed enrichment of Rh near the NP surfaces and Pd in the cores (Figure 2, bottom). The extent of segregation was nowhere near what might be expected for a transition to a fully segregated core–shell structure. However, this observation is in agreement with the XPS data for 3 h μwI-RhPd NPs, which indicated a slight increase in the Rh content, as the X-ray penetration depth may have been impeded by the native PVP overlayers and this would have resulted in selective probing of the NP peripheries.

The vapor-phase hydrogenation of cyclohexene (CHE) to cyclohexane (CHA) in continuous-flow mode was used as a model reaction to explore the catalytic activity of the RhPd NPs versus that of their monometallic counterparts. Catalysts were prepared by supporting Rh, Pd, and RhPd NPs on amorphous silica, and the resulting composites were mixed thoroughly with sand before loading the catalyst materials into a fixed-bed reactor setup (Scheme S12). Notably, the supported composite catalysts are highly active hydrogenation catalysts without the need for harsh pretreatment (calcination to remove the PVP capping agent). Activation was simply achieved by flowing a H_2/He mixture (1:1.5) over the catalyst at 25 °C for 30 min. Subsequent introduction of CHE vapor into the gas stream initiated catalysis; the products were monitored on-stream at 3.5 min intervals by gas chromatography (GC) with a pneumatically gated automated sampling valve.

Pertinent catalysis results obtained at 25 °C are presented in Figure 3; additional results from both the μwI- and CvH-NPs are also given in Figure S13. After 5 h on-stream, the μwI-RhPd NPs exhibited steady-state turnover frequency (SS-TOF) values of 8.5 and 8.2 surface $site^{-1}\,s^{-1}$ for synthesis times of 30 s and 3 h, respectively. This result is important in demonstrating that there is virtually no catalytic benefit to longer NP synthesis times and that active catalysts can be prepared in only 30 s. Both catalysts showed remarkably stable activity under the reaction conditions, and they retained approximately 73% of their initial TOF, even after 5 h on-stream. The corresponding CvH-RhPd NPs displayed higher initial TOFs, but the values de-

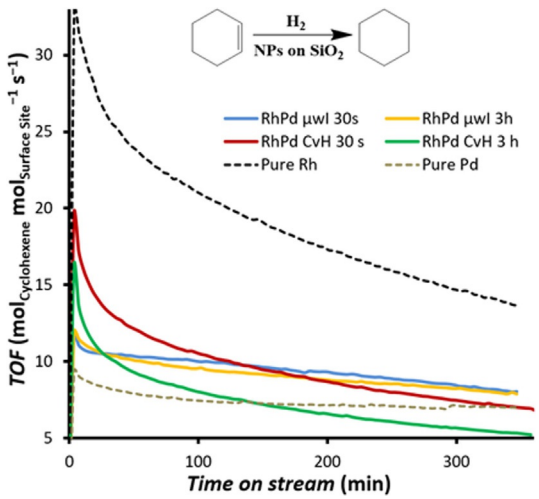

Figure 3. Average TOF values observed for the hydrogenation of cyclohexene by Rh, Pd, and representative μwI- and CvH-RhPd NPs.

cayed much more rapidly and fell below the TOFs of their microwave-irradiated counterparts in less than 150 min. This type of behavior is commonly ascribed to NPs that are initially structurally less isotropic with a greater proportion of higher energy facets that are subsequently lost by adsorbate-induced restructuring processes. If compared with microwave-irradiation-prepared monometallic Rh and Pd NPs, the μwI-RhPd NPs are more active than Pd (SS-TOF = 7.1 s^{-1} at 5 h) but are not as active as Rh (SS-TOF = 13.6 s^{-1} at 5 h). However, the more-active Rh NPs continued to show significant deactivation at 5 h; owing to its high adsorption reactivity, Rh is well known to be more vulnerable to deactivation by coking than Pd. It is therefore plausible that the presence of Pd in the alloy NPs reduces the extent of deactivation. No agglomeration of the particles was observed by TEM for any of the catalysts after 6 h of hydrogenation (Figure S15).

Previously, we reported that H and CHE binding energies could be used as descriptors to evaluate the catalytic performance of hydrogenation catalysts.[15] A volcano-shaped activity plot shows that the H binding energies on both Rh(111) and Pd(111) are too strong to reach the highest TOF activity.[15,27] To understand the experimental results of this study, DFT calculations were performed to calculate the H and CHE binding energies on Rh(111), Pd(111), and RhPd(111) random alloy surfaces. Details of the calculations are provided in the Supporting Information. Figure 4a shows the calculated average H binding energies at four triatomic ensembles (threefold hollow sites consisting of Rh_3, Rh_2Pd_1, Rh_1Pd_2, or Pd_3) on $Rh_{0.50}Pd_{0.50}$, whereas Figure 4b shows the calculated average CHE binding energies at five additional binding sites (Rh_1 or Pd_1 atop sites; Rh_2, RhPd, or Pd_2 twofold bridge sites). These binding modes were chosen as the most favorable modes on the basis of extensive single-crystal studies performed on (111) noble-metal surfaces in ultrahigh vacuum.[32] The results indicate that the binding of CHE is strongest to Rh, weakest to Pd, and changes roughly linearly with binding site composition in the $Rh_{0.50}Pd_{0.50}$ alloy. The binding of H is somewhat more complicated; it is stronger on the Pd(111) surface than on the Rh(111) surface. In the $Rh_{0.50}Pd_{0.50}$ alloy, however, H binding is stronger to Rh atoms and weaker to Pd atoms. This somewhat counterintuitive result can be explained by the electronic or "ligand" effect, for which Pd atoms that surround the Rh-rich sites have the effect of increasing the H binding strength, whereas Rh atoms that surround the Pd-rich sites decrease the strength of H binding. This is a consequence of charge transfer from Rh to Pd in the alloy.[33] Additional calculations demonstrating the correlation between binding site composition and H binding energy are shown in Figures S20 and S21.

The H binding energy of Rh is closer to the top of the volcano than that of Pd, as shown in Figure 4c.[15,27] Whereas Pd has a more suitable binding energy for CHE, the overall predicted hydrogenation activity is lower than that for Rh. The average binding energies of H and CHE on the $Rh_{0.50}Pd_{0.50}$ alloy (111) surface are intermediate between those on Rh and Pd, as one would expect from the trends in Figure 4a,b. These theoretical results are consistent with the experiments and show that the CHE hydrogenation activity is of the order Rh > $Rh_{0.50}Pd_{0.50}$ > Pd.

In conclusion, poly(vinylpyrrolidone)-capped RhPd nanoparticles (NPs) with randomly alloyed structures could be rapidly synthesized by using microwave-assisted heating with ethylene

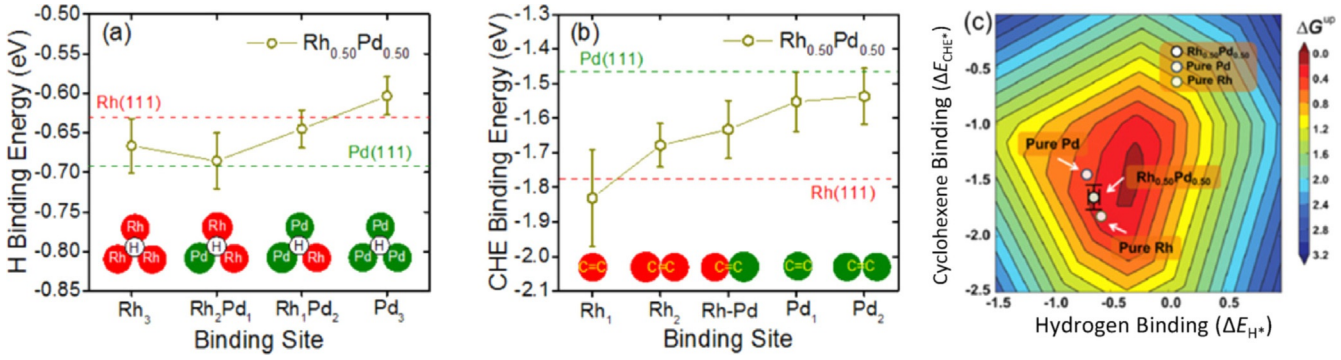

Figure 4. Average a) H binding energies at four triatomic ensembles and b) CHE binding at three bridging and two atop sites on the (111) surface of a slab model of the $Rh_{0.50}Pd_{0.50}$ alloy. The horizontal dashed lines indicate the binding energies on Rh(111) and Pd(111). The insets show the ensembles and molecular binding geometries. The error bars indicate the standard deviation of binding energies calculated from 10 different random alloy geometries. c) Volcano plot showing the hydrogenation activity of $Rh_{0.50}Pd_{0.50}$ as predicted by two descriptors: the H and CHE binding energies. Pure Rh is closest to the volcano peak, with the highest predicted activity, followed by $Rh_{0.50}Pd_{0.50}$, and then Pd.

glycol as both the solvent and the reducing agent. The RhPd NPs with near equimolar compositions made in the shortest reaction time of 30 s were active and stable gas-phase alkene hydrogenation catalysts if supported on amorphous silica without the need for pretreatment. Relative to the catalytic activities of the pure Rh and Pd NP catalysts, the catalytic activity of the RhPd NPs was intermediate, but these NPs showed improved steady-state behavior. The observed findings were in good agreement with DFT calculations on the basis of modulating the hydrogen and cyclohexene surface binding energies through Rh–Pd charge-transfer effects.

Experimental Section

The method used to synthesize the RhPd alloy NPs was a variation of the one described by García et al.[15] $RhCl_3{\cdot}xH_2O$ (10 mg, 0.048 mmol) was dissolved in ethylene glycol (EG, 2.5 mL) by sonication, and then this solution was used to dissolve K_2PdCl_4 (16 mg, 0.049 mmol). Separately, poly(vinylpyrrolidone) (PVP, 200 mg) was dissolved in EG (15 mL) in a 50 mL round-bottomed flask, and the solution was heated to 165 °C in a CEM MARS 5 programmable microwave chamber; for a more detailed description see Figure S1. Once the target temperature had been reached, the precursor solution was injected at 320 mL h^{-1} (12.5 mmol h^{-1}) by using a programmable syringe pump. After the injection was complete, heating was continued for 30 s, 3 min, 30 min, or 3 h before the reaction was quenched in an ice water bath. The product was washed by using a two-stage process. First, the product was precipitated by diluting each half of the reaction solution with acetone (30 mL) and then centrifuged at 5500 rpm for 5 min. Second, the black product in each centrifuge tube was redispersed in ethanol (5 mL) before it was reprecipitated with hexanes (30 mL) and centrifuged at 5500 rpm for 5 min; this ethanol/hexanes wash was performed a total of two times. The final product was dried overnight in a vacuum desiccator. For comparison, RhPd NPs were also made by conventional oil-bath heating by using the same conditions described above. Monometallic Rh and Pd NPs were synthesized as controls by using the method reported by Dahal et al.[30] To obtain similarly sized NPs from both microwave irradiation and conventional heating, a secondary injection of the Rh precursor was performed in the CvH-Rh synthesis to aid further growth; the initial seeding injections were sufficient for the other catalysts.

Acknowledgements

The authors thank Drs. Dwight Romanovicz and Karalee Jarvis for TEM analytical assistance. Funding for this research was provided by the National Science Foundation under Grant No. CHE-1505135 and the Welch Foundation (Grant Nos. F-1738 (S.M.H.) & F-1831 (G.H.)).

Conflict of interest

The authors declare no conflict of interest.

Keywords: alloys · hydrogenation · nanoparticles · palladium · rhodium

[1] J. D. Burrington, *Industrial Catalysis: Chemistry and Mechanism*, Imperial College Press, London, **2016**.
[2] K. C. Taylor, *Catal. Rev.* **1993**, *35*, 457–481.
[3] L. Yin, J. Liebscher, *Chem. Rev.* **2007**, *107*, 133–173.
[4] N. R. Shiju, V. V. Guliants, *Appl. Catal. A* **2009**, *356*, 1–17.
[5] B. Yoon, C. M. Wai, *J. Am. Chem. Soc.* **2005**, *127*, 17174–17175.
[6] X.-R. Ye, Y. Lin, C. Wang, M. H. Engelhard, Y. Wang, C. M. Wai, *J. Mater. Chem.* **2004**, *14*, 908–913.
[7] R. Schlögl, *Angew. Chem. Int. Ed.* **2015**, *54*, 3465–3520; *Angew. Chem.* **2015**, *127*, 3531–3589.
[8] J. A. Johnson, J. J. Makis, K. A. Marvin, S. E. Rodenbusch, K. J. Stevenson, *J. Phys. Chem. C* **2013**, *117*, 22644–22651.
[9] P. Fröhlich, T. Lorenz, G. Martin, B. Brett, M. Bertau, *Angew. Chem. Int. Ed.* **2017**, *56*, 2544–2480; *Angew. Chem.* **2017**, *129*, 2586–2624.
[10] D. Astruc, F. Lu, J. R. Aranzaes, *Angew. Chem. Int. Ed.* **2005**, *44*, 7852–7872; *Angew. Chem.* **2005**, *117*, 8062–8083.
[11] T. P. Bigioni, X. M. Lin, T. T. Nguyen, E. I. Corwin, T. A. Witten, H. M. Jaeger, *Nat. Mater.* **2006**, *5*, 265–270.
[12] N. R. Jana, L. Gearheart, C. J. Murphy, *Chem. Mater.* **2001**, *13*, 2313–2322.
[13] T. K. Sau, C. J. Murphy, *J. Am. Chem. Soc.* **2004**, *126*, 8648–8649.
[14] Y. G. Sun, Y. N. Xia, *Science* **2002**, *298*, 2176–2179.
[15] S. García, L. Zhang, G. W. Piburn, G. Henkelman, S. M. Humphrey, *ACS Nano* **2014**, *8*, 11512–11521.
[16] H. Kobayashi, K. Kusada, H. Kitagawa, *Acc. Chem. Res.* **2015**, *48*, 1551–1559.
[17] K. Kusada, H. Kobayashi, R. Ikeda, Y. Kubota, M. Takata, S. Toh, T. Yamamoto, S. Matsumura, N. Sumi, K. Sato, K. Nagaoka, *J. Am. Chem. Soc.* **2014**, *136*, 1864–1871.
[18] K. Kusada, M. Yamauchi, H. Kobayashi, H. Kitagawa, *J. Am. Chem. Soc.* **2010**, *132*, 15896–15898.
[19] P. Kunal, E. J. Roberts, T. Carson, K. Jarvis, N. Malmstadt, R. L. Brutchey, S. M. Humphrey, *Chem. Mater.* **2017**, *29*, 4341–4350.
[20] S. N. Tripathi, S. R. Bharadwqi, *J. Phase Equilib.* **1994**, *15*, 208–212.
[21] H. Noh, T. B. Flanagan, B. Cerundolo, A. Craft, *Scr. Metall. Mater.* **1991**, *25*, 225–230.
[22] H. Noh, J. D. Clewley, T. B. Flanagan, A. P. Craft, *J. Alloys Compd.* **1996**, *240*, 235–248.
[23] A. K. M. Fazle Kibria, Y. Sakamoto, *Int. J. Hydrogen Energy* **2000**, *25*, 853–859.
[24] E. R. Essinger-Hileman, D. DeCicco, J. F. Bondi, R. E. Schaak, *J. Mater. Chem.* **2011**, *21*, 11599–11604.
[25] H. Kobayashi, H. Morita, M. Yamauchi, R. Ikeda, H. Kitagawa, Y. Kubota, K. Kato, M. Takata, S. Toh, S. Matsumura, *J. Am. Chem. Soc.* **2012**, *134*, 12390–12393.
[26] S. García, G. W. Piburn, S. M. Humphrey in *Microwave-assisted Synthesis of Metallic Nanoparticles, In Microwave Engineering of Materials—From Mesoscale to Nanoscale* (Ed.: Erwann Guenin), Pan Stanford Publishing, Singapore, **2016**.
[27] P. Kunal, H. Li, B. L. Dewing, L. Zhang, K. Jarvis, G. Henkelman, S. M. Humphrey, *ACS Catal.* **2016**, *6*, 4882–4893.
[28] J. D. Hoefelmeyer, K. Niesz, G. A. Somorjai, T. D. Tilley, *Nano Lett.* **2005**, *5*, 435–438.
[29] Y. Xiong, J. Chen, B. Wiley, Y. Xia, Y. Yin, Z.-Y. Li, *Nano Lett.* **2005**, *5*, 1237–1242.
[30] N. Dahal, S. García, J. Zhou, S. M. Humphrey, *ACS Nano* **2012**, *6*, 9433–9446.
[31] P. Scherrer, *Nachr. Ges. Wiss. Goettingen Math.-Phys. Kl.* **1918**, *2*, 98–100.
[32] T. T. T. Hanh, Y. Takimoto, O. Sugino, *Surf. Sci.* **2014**, *625*, 104–111.
[33] W. Tang, G. Henkelman, *J. Chem. Phys.* **2009**, *130*, 194504.

Manuscript received: July 12, 2017
Accepted manuscript online: July 14, 2017
Version of record online: September 14, 2017